Published in final edited form as:
J Neurosci Methods. 2011 January 30; 195(1): 36–46. doi:10.1016/j.jneumeth.2010.11.014.

Chronic in vivo multi-circuit neurophysiological recordings in mice

Kafui Dzirasa[1,2,5,*], **Romulo Fuentes**[3,7], **Sunil Kumar**[1], **Juan M. Potes**[3], and **Miguel A. L. Nicolelis**[3,4,5,6,7]

[1] Dept. of Psychiatry and Behavioral Sciences, Duke University Medical Center, Durham, North Carolina 27710

[2] Duke Institute of Brain Sciences, Duke University Medical Center, Durham, North Carolina 27710

[3] Dept. of Neurobiology, Duke University Medical Center, Durham, North Carolina 27710

[4] Dept. of Psychology and Neuroscience, Duke University Medical Center, Durham, North Carolina 27710

[5] Center for Neuroengineering, Duke University Medical Center, Durham, North Carolina 27710

[6] Dept. of Biomedical Engineering, Duke University Medical Center, Durham, North Carolina 27710

[7] Edmond and Lily Safra International Institute of Neuroscience of Natal (ELS-IINN), Natal, Brazil

Abstract

While genetically modified mice have become a widely accepted tool for modeling the influence of gene function on the manifestation of neurological and psychiatric endophenotypes, only modest headway has been made in characterizing the functional circuit changes that underlie the disruption of complex behavioral processes in various models. This challenge partially arises from the fact that even simple behaviors require the coordination of many neural circuits vastly distributed across multiple brain areas. As such, many independent neurophysiological alterations are likely to yield overlapping circuit disruptions and ultimately lead to the manifestation of similar behavioral deficits. Here we describe the expansion of our neurophysiological recording approach in an effort to quantify neurophysiological activity across many large scale brain circuits simultaneously in freely behaving genetically modified mice. Using this expanded approach we were able to isolate up to 70 single neurons and record local field potential (LFP) activity simultaneously across 11 brain areas. Moreover, we found that these neurophysiological signals remained viable up to 16 months after implantation. Thus, our approach provides a powerful tool that will aid in dissecting the central brain network changes that underlie the complex behavioral deficits displayed by various genetically modified mice.

Keywords

Chronic; mice; multi-site; neurophysiology; single unit; LFP

[*]Corresponding Author: Kafui Dzirasa, M.D. Ph.D., Department of Psychiatry and Behavioral Sciences, Duke University Medical Center, 333 Bryan Research Building, Durham, NC 27710, USA, kafui.dzirasa@duke.edu.

Research Highlights

- Whole Circuit recordings in mice
- Chronic multi-site implants
- Dynamic oscillatory activity across circuits

Introduction

Genetically modified (GM) mice have become a widely accepted tool for modeling the influence of gene function on behavior (Ekstrand et al., 2007; Giros et al., 1996; Mohn et al., 1999; Roybal et al., 2007; Welch et al., 2007); however, only modest headway has been made in characterizing the functional changes that underlie the disruption of complex behavioral processes observed across various models. The central challenge lies within the fact that many of the GM mouse lines used to model central nervous system (CNS) disorders display alterations in genes that are expressed across multiple brain areas. Furthermore, even in cases where genetic manipulations are restricted to singe brain regions, these targeted manipulations have been shown to induce secondary changes across other brain areas (Kellendonk et al., 2006). Finally, since even simple behaviors require the activation of neural networks which span multiple brain regions, many different isolated brain changes are likely to be sufficient to alter circuit function and ultimately facilitate similar gross behavioral deficits. Taken together, these challenges present a major obstacle to identifying the specific genetic manipulation-induced brain changes that directly underlie the manifestation of a particular set of circuit deficits and ultimately behavioral dysfunction.

In vivo neurophysiological recordings have become an emerging tool for probing the functional molecular components of brain oscillatory networks in various GM mouse models during freely-moving behavior (Dzirasa, 2008). For example, genetic disruption of the 5-HT1A receptor potentiates hippocampal theta (4–11Hz) oscillatory activity during anxiety related task performance (Gordon et al., 2005). Moreover, genetic disruption of the dopamine transporter (DAT) potentiates hippocampal gamma (30–50Hz) oscillatory activity during exploration of a novel environment (Dzirasa et al., 2006), and diminishes peak hippocampal theta oscillatory frequencies in the home cage and during REM sleep (Dzirasa et al., 2009b). Knock-out (KO) mice for the gap junction protein Connexin-36 have also been shown to display impairments in hippocampal gamma oscillatory coordination (Buhl et al., 2003), and in an elegant gene by drug interaction study, the targeted activation of genetically modified M3 cholinergic receptors has been shown to induce hippocampal gamma oscillatory activity (Alexander et al., 2009). Notably, *in vivo* recordings have also been utilized to investigate how selective gene manipulations alter neuronal firing rates and firing patterns in freely behaving mice (Adhikari et al., 2010; Alexander et al., 2009; Costa et al., 2006; McHugh et al., 2007; Zweifel et al., 2009).

Since the induction of behavior requires the activation of neural circuits spanning multiple brain regions, an emerging number of studies have been geared towards probing circuit function in GM mice via *in vivo* neurophysiological recordings conducted simultaneously across multiple brain areas. For example, it has been shown that acute dopamine depletion in mice lacking the dopamine transporter induces the synchronization of cortical-striatal ensembles (Costa et al., 2006). Moreover, studies have shown that mice genetically engineered to display NMDA receptor hypofunction exhibit enhanced hippocampus-prefrontal cortex inter-area theta-gamma coupling, and diminished intra-area theta-gamma coupling (Dzirasa et al., 2009a). More recently, an elegant behavioral study demonstrated

that hippocampus and prefrontal cortex theta oscillations synchronize during anxiety related behaviors, and that genetic disruption of the 5-HT1A receptor alters network processing across the hippocampal-prefrontal cortex pathway (Adhikari et al., 2010). Altogether, these studies demonstrate the utility of *in vivo* recordings in probing circuit deficits underling the behavioral manifestations seen in various lines of transgenic mice, and highlight the need for the development of tools which allow investigators to record more neurons per mouse and neural activity across entire brain circuits concurrently.

Materials and Methods

Animal Care and Use

Mice were separated into individual cages maintained in a humidity and temperature-controlled room with water available *ad libitum*, and surgically implanted with recording electrodes at 2–5 months. Recordings were initiated following a 2–4 week recovery period. All neurophysiological recordings were conducted in an 11″ × 11″ open field test environment.

All studies were conducted with approved protocols from the Duke University Institutional Animal Care and Use Committee and were in accordance with the NIH guidelines for the Care and Use of Laboratory Animals.

Surgery

Mice were anesthetized with ketamine (100mg/kg) and xylazine (10mg/kg), placed in a stereotaxic device, and ground screws were secured to the anterior cranium and above cerebellum. Microwires were arranged in array bundles (see results for description of bundles), and surgically implanted based on stereotaxic coordinates measured from bregma. The following coordinates were used for experiments presented in this manuscript (all coordinates are measured from bregma):

Area	AP (mm)	ML (mm)	DV (mm)
Ventral Striatum	+1.25	+1.15	−4.0
Amygdala	−1.6	−2.5	−4.8
Fr_Association_Cx	+2.95	−1.5	−0.5
Hippocampus	−2.3	+1.75	−1.2
Motor Cortex	+1.2	−1.75	−0.5
Prelimbic_Cx	+2.5	+0.25	−0.75
Orbital_Fr_Cx	+2.6	−1.1	−1.7
Medial Dorsal Thalamus	−1.6	+0.3	−2.9
Ventral Posterior Thalamus	−1.0	−1.1	−3.3
D.L. Striatum	+0.6	−2.0	−2.0
Substantia Nigra	−3.2	−1.35	−4.2
VTA	−3.2	+0.3	−4.25

Microarray bundles targeting brain areas that were closest to the ground screws were implanted first. These implants were anchored to three screws using dental acrylic, and successive microwire bundles were anchored to these implants. Exposed microwires were covered, and electrode bases were fixed to microwire bundle implants using Instacure-2000

cyanoacrylate (Hobbylinc.com, IC-2000). For experiments with integrated electromyographic recordings, tungsten EMG wires built directly into the PC boards were also placed in trapezius, triceps, and/or whisker muscle, and skin was closed using surgical sutures.

Neuronal and LFP Data acquisition

Neuronal activity was recorded using the Multi-Neuron Acquisition Processor system (Plexon Inc, TX), and activity was initially sorted using an online sorting algorithm (Plexon Inc, TX). Only cells that had a clearly identified waveform with a signal-to-noise ratio of at least 2:1 on the oscilloscope were used. To confirm the quality of the recorded cells, they were sorted offline using an algorithm based on PCA cluster analysis (Offline Sorter, Plexon Inc). All cells were presented in neuron isolation counts; however, only clearly defined cell clusters with clear refractory periods on the interspike-interval histogram (larger than 1.3 ms in this study) were used for PCP analysis.

Local field potentials (LFPs) were preamplified (500X), filtered (0.5–400 Hz), and digitized at 500 Hz using a Digital Acquisition card (National Instruments, Austin, TX) and a Multi-Neuron Acquisition Processor (Plexon, Dallas, TX). DC coupled headstages were used for neurophysiological recordings, and all recordings were referenced to two of the implanted screws. It is important to note that LFP recordings were associated with a significant phase offset that varied across frequencies (Nelson et al., 2008). These fixed phase offsets were corrected using the LFPAlign software (Plexon, Dallas, TX).

Determination LFP oscillatory power and cross-structure synchrony

LFPs were filtered using butterworth bandpass filters designed to isolate either 1–4Hz, 4–8Hz, 8–14Hz, 14–30Hz, or 30–55Hz oscillations. The instantaneous amplitude and phase of the filtered LFPs were then determined using the Hilbert transform and oscillatory power within each frequency range was determined for each LFP by taking the mean of the amplitude envelope calculated for each of the filtered LFP traces. Cross- structure coherence was calculated on local field potential recording pairs using the Matlab *mscohere* function at a 2 second sliding window with a 0.5 second step. This process yielded an average coherence value, ranging from 0 to 1, for each brain-area pair of interest.

Electrophysiological recording in mice treated with PCP

Mice were treated with saline 4 weeks after surgical implantation, and subject to recordings in a novel environment. Following an initial 30 minute baseline recording period, mice were treated with PCP (3 mg/kg, i.p.) and neurophysiological data was recorded for an additional 30 minutes. The 10 minute periods beginning 10 minutes after saline or drug treatments were used for all analysis presented in this manuscript. In order to determine the effects of PCP on within-area population firing rates, we generated a mean firing-rate distribution for each area across the 10 minute recording segments (30s bins) and calculated the 99% confidence interval based on a Poisson distribution. We considered that a population of neurons changed their firing rate if the mean population firing rate following PCP treatment was outside of the 99% confidence interval observed during the previous recording period (i.e., the PCP was compared to baseline saline recording period).

Results

In order to increase the number of neurons that we could acquire from each mouse, we set out double the number implanted microwires to 64. Our initial approach entailed implanting four multiwire electrode arrays (16-microwire arrays) in each mouse. While we have used this approach successfully in the past to increase the number of neurons isolated in rats and

non-human primates (Nicolelis et al., 2003; Nicolelis et al., 1997), we found that this approach did not work in mice. Each implanted electrode covered a cranial surface area of approximately 12mm^2, and electrodes required a minimal separation of approximately 3mm for headstages to be attached during neurophysiological recordings. Since the total cranial window available for implantation in mice was ~50mm^2 (after accounting for anchoring screws), the number of electrodes (and thus brain areas) that we could implant per mouse was limited to three. To overcome this limitation, we designed novel electrodes where microwire bundles remained free floating from the electrode base (Figure 1A–B). This simple design modification allowed us to implant microwire bundles with a minimal separation of <1mm, and headstages and connectors could be fixed adjacent to the implanted microwire bundles on the side of the animal's head (Figure 1C–D). Since only the implanted microwire bundles were located directly above the cranium, up to 64 microwires arranged in many array bundles could be implanted in a single mouse. Heretofore, we describe several electrode designs and experimental applications enabled by this approach. Importantly, with the exception of the simple floating design modification, the construction and implantation of these floating bundle electrodes differed in no way from our previously described fixed bundle designs (Dzirasa, 2008).

We created several high-density microwire array designs where single-wire electrodes were arranged to sample neuronal activity throughout the thickness of brain tissue (Figure 2A–C). Using this approach, we were able to implant up to 32 wires in a single brain area (recorded bilaterally) and isolate on average 22 neurons/area (Table 1). Two high-density arrays were implanted per animal for a total of 64 microwire channels/mouse. The total weight of the implant was 2.2 grams, and we found that mice could tolerate implants that weighed up to 10% of their free feeding body weight. Next, we designed high-density microwire arrays to sample brain activity across two brain areas simultaneously. Our initial implants targeted primary motor cortex (M1) and dorsolateral striatum (DLS) simultaneously using 32 microwire arrays with 16 microwires staggered in the dorsal ventral direction by approximately 1.5–1.3mm (Figure 3A–B). Using this approach, we found that we could isolate on average 58 neurons/mouse (see Figure 3C, and Table 2). This represented approximately twice the number of neurons that we were able to isolate in our previous studies (Costa et al., 2006).

After successfully increasing the number of neurons we could record from a freely behaving mouse, we set out to isolate activity across a set of areas constituting a large-scale brain circuit. Thus, we targeted the four brain areas (prelimbic cortex, ventral striatum, medial dorsal thalamus, and ventral tegmental area [VTA], see Figure 4A–B) comprising the dopamine reward circuit by implanting a novel microwire array with a flexible satellite bundle design. Using this approach we were able to isolate the simultaneous activity of up to 73 neurons and LFPs across the dopamine reward circuit simultaneously (Figure 4C and Table 3). Next, we tested if our approach could be used to dissect the effect of psychoactive agents on neurophysiological brain networks in freely behaving mice. As a proof of principle, we quantified the effect of a well established drug of abuse, phencyclidine (PCP, 3 mg/kg i.p.), on neurophysiological activity recorded across the dopamine reward circuit and a motor circuit simultaneously. For these experiments, we used an additional group of mice implanted in prelimbic cortex, ventral striatum, VTA, M1, and DLS (Figure 5A). We found that treatment with PCP increased 1–4Hz (delta) oscillatory power in V. Striatum, and 4–8Hz (theta) oscillatory power across all of the brain areas observed (Table 4). Treatment with PCP also decreased 14–30Hz (beta) oscillatory power in DLS and VTA, and 30–55Hz (gamma) oscillatory power in V. Striatum, DLS and M1 (Figure 5B). Notably, the strongest effects of PCP on delta, theta, and gamma power were observed in V. Striatum (~40% change in oscillatory power for each frequency, Table 4). Since multiple studies have indicated that cross-structural neural synchrony reflects the activation of distributed neural

networks (Adhikari et al., 2010; Dzirasa et al., 2010b; Fell et al., 2001; Jones and Wilson, 2005; Rodriguez et al., 1999; Seidenbecher et al., 2003), we also quantified the effect of PCP on this measure. Our results indicated that the dopamine reward and motor circuits examined were characterized by three bands of high cross-structural coherence (1–6Hz, 10–25Hz, and 30–55Hz, Figure 5C). Moreover, we found that treatment with PCP enhanced 1–6Hz coherence across the dopamine reward circuit (but not the motor circuit), and decreased 30–50Hz coherence across all of the circuits examined. Treatment with PCP also increased the single neuron population firing rates across DLS and VTA, and decreased the single neuron population firing rate across M1 and PrL_Cx (Figure 5D). Together, these findings suggested that in principle our approach could be used as a method to dissect the effect of psychoactive agents on neurophysiological brain networks in GM mice.

In a further step, we engineered a light weight electrode design to target multiple brain circuits simultaneously. For the initial electrode design, we used a total of 32 microwires to target prelimbic cortex, orbital frontal cortex, ventral striatum, VTA, ventral thalamus, primary motor cortex, primary sensory cortex, and DLS (Figure 6A). We also modified our microwire bundle designs in order to target multiple brain areas simultaneously with a single bundle (Figure 6B). Our single-electrode design reduced the weight of the total implant to 1.6 grams, allowing us to implant animals as light as 16 grams. This approach may be especially suitable for younger mice, or genetic mutations that yield smaller mice lines. While this approach reduced the total number of neurons recorded per mouse compared to our previous designs, we were able to record neural activity across all of the implanted areas (see Figure 6D, and Table 6). Notably, when we performed serial recordings in implanted mice, we found that the number of neurons isolated per mouse doubled between 2 and 8 weeks after implantation (Figure 7). Incidentally, we also tested several electrode designs that allowed us to simultaneously record electromyographic (EMG) activity (Figure 8).

Finally, we designed microwire electrodes to probe large-scale neural networks (see Figure 9A). Using this approach, we were able to record neural oscillatory activity across 11 brain areas simultaneously (ventral striatum, amygdala, frontal association cortex, hippocampus, M1, orbital frontal cortex, prelimbic cortex, substantia nigra, DLS, thalamus, and VTA) in freely behaving mice (Figure 9B–C). Notably, the number of brain areas implanted was only limited by the amount of cranial surface area available for implantation and could be increased further with modification to the design of individual microwire bundles. We were also able to isolate up to 40 single neurons/mouse across the 11 implanted brain areas (Figure 9D). Since the attributes of the data obtained by our method were especially well suited for cross-structural neural synchrony studies (i.e. large number of LFPs recorded simultaneously across many brain areas), we used coherence analysis to examine the cross-structural synchrony profiles of the 11 implanted brain areas. Surprisingly, our results indicated that cross-structural neural synchrony patterns differed widely across the brain area pairs used for coherence analysis (Figure 10). For example, amygdala tended to synchronize with ventral striatum and VTA in the gamma frequency range, while hippocampus tended to synchronize with amygdala and thalamus in the theta frequency range. Additionally, some brain areas pairs displayed low overall synchrony (i.e., thalamus and frontal association cortex), while others displayed high synchrony across all frequencies (i.e., thalamus and substantia nigra). Together these results demonstrated that our approach was capable of characterizing the dynamic neural interactions which define widely distributed brain circuits. When we examined the stability of our neural and neuronal signals across each of the 11 brain areas, we found that neural signals were still viable more than a year after electrode implantation (n=2 mice, Figure 11). Moreover, we were able to isolate neuronal signals more than a year after implantation as well (Table 7). Importantly, these results suggest that neurophysiological signals recorded using our recording approach are likely to be viable for the entire lifespan of implanted mice.

Discussion

GM mice have become a widely accepted tool for modeling the influence of gene function on behavior (Ekstrand et al., 2007; Giros et al., 1996; Mohn et al., 1999; Roybal et al., 2007; Welch et al., 2007); however, only modest headway has been made in characterizing the functional brain changes that underlie the disruption of complex behavioral processes observed across various models. Since these behavioral deficits ultimately result from changes in neural circuits which span multiple brain regions, we have created an approach that allows brain activity to be probed across multiple large-scale brain circuits simultaneously in freely behaving GM mouse models of neuropsychiatric illness. Our findings indicate that our expanded neurophysiological recording approach is capable of isolating up to 70 single neurons in a single freely behaving mouse. This represents a 2–3 fold increase over the number of single neurons previously isolated in freely behaving mice using our classic neurophysiological recording techniques. We also demonstrate that our technique can be used to acquire local field potential and unit activity across 11 brain areas simultaneously in freely behaving mice, though this approach yields a diminished number of units that can be isolated from each implanted brain area. Local field potentials, on the other hand, can be isolated from each recording wire implanted in each brain area yielding a maximum total 64 continuous signals/mouse. Moreover, we show that these signals remain viable for over 12 months after implantation.

LFP's are classically considered inferior neurophysiological signals compared to single units since LFP's are subject to signal artifacts that may result from gross volume conduction, electrophysiological noise introduced from referencing sites (i.e. ground screws, 60Hz artifact), or background noise generated during behaviors such as chewing, yawning, and grooming (not to mention others). However, our multi-circuit recording approach has the potential to overcome many of these limitations. First, electrophysiological and background noise would vary equivalently across time in all of the simultaneously recorded LFP signals. Thus, algorithms can be developed to isolate these aberrant signals and filter them appropriately across channels. Second, one can determine if recorded LFP signals result from pertinent neurophysiological interactions or simply volume conduction since our approach allows neurophysiological activity to be acquired simultaneously across brain areas located throughout the brain (various depths and rostral-caudal locations). Thus, LFP signals that result from volume conduction will generate spectral synchrony between LFP pairs that is also observed in LFP signals recorded intermediate to the two LFP pairs of interest. An example of this approach is demonstrated in our recent study where we showed that acute depletion of norepinephrine differentially affects orbital frontal cortex-striatal delta coherence and frontal association cortex-striatal delta coherence despite the fact that the cortical electrodes were located ~1mm apart (Dzirasa et al., 2010a). Finally, our findings also provide evidence that our approach can overcome limitations in analysis that result from behavioral noise (i.e. movement artifacts). For example, our findings demonstrated that treatment with PCP differentially affects motor and reward circuits (as measured via inter-area coherence), despite the increased behavioral profiles induced by treatment with the PCP. While movement artifacts are not necessarily equally present across all LFP channels, these signals vary equivalently across LFP channels across time and ultimately generate spectral coherence that varies equivalently and not differentially across LFP pairs.

One of the most notable findings observed using our multi-circuit (>10 simultaneously recorded bran areas) approach is that different brain areas tend to synchronize in different frequency ranges. For example, V. Striatum tends to synchronize with Amygdala and V. Striatum in the gamma frequency range, while hippocampus tends to synchronize with Amygdala and Thalamus in the theta frequency range. Thus our approach provides a

powerful tool that can be potentially used to dissect the neural oscillatory modes underling circuit level interactions across specific brain networks.

Multiple *in vivo* electrophysiological studies have been conducted in rodents in an effort to study the effect of drugs of abuse on brain function. For example, it has been shown that cocaine-seeking behavior is encoded in the core and shell of nucleus accumbens (Carelli et al., 2000; Owesson-White et al., 2009). Moreover, repeated cocaine exposure has been shown to abolish the presence of membrane bi-stability normally present in neurons located in the limbic prefrontal cortex (Trantham et al., 2002). Nevertheless, the approaches used in these studies were severely limited in their ability to identify and characterize the dynamic brain network changes that underlie the manifestation of addiction-related behaviors since they only acquired brain activity across a small number of brain areas at a time. Our findings observed in mice treated with PCP provide evidence that drugs of abuse induce a wide array of changes that vary across brain circuits. For example, our results showed that treatment with PCP increased the population firing rate of DLS and VTA neurons, and decreased the population firing rate of M1 and PrL_Cx neurons. On the other hand, treatment with PCP had no effect on the population firing rate of V. Striatal neurons. Treatment with PCP also induced differential changes at the level of circuit synchrony. For example, PCP enhanced 1–6Hz spectral coherence across the entire dopamine reward circuit, but not the motor circuit, and reduced gamma spectral coherence across both of the circuits examined. Together, this demonstrates that drugs of abuse induce a diverse array of circuit level changes across different brain networks. Notably, since neurophysiological signals can be acquired in freely behaving mice more than a year after their initial surgical implantation, our neurophysiological recording approach serves as a powerful tool that can be used to simultaneously examine multiple circuit level changes underlying the acquisition, expression, and extinction of addiction related behaviors. Several GM mouse line have been shown to display altered behavioral responses to drugs of abuse. For example, mice with an N-ethyl-N-nitrosurea induced point mutation in the circadian gene *Clock* (*Clock*-Δ19 mice) have been shown to display increased sensitivity to rewarding stimuli including cocaine (Roybal et al., 2007), while mice lacking a phosphoprotein downstream of D1 and D2 dopamine receptors (DARPP-32 KO mice) have been shown to display a diminished behavioral response to Amphetamine, PCP, and LSD (Svenningsson et al., 2003). Thus, our approach provides a powerful tool that can be used with these GM models to dissect how changes in gene and protein expression alter neurophysiological circuits responsible for the acquisition and expression of addition related behaviors.

Conclusion

Overall, our chronic neurophysiological recording approach provides a powerful tool for dissecting the circuit changes underlying behavioral changes seen various GM mouse models of neurological and psychiatric diseases and probing the effect of pharmacological agents on these circuits. Moreover, our recording approach can potentially be integrated with novel optogenetic and chemicogenetic tools capable of manipulating neuronal activity in order to quantify the role that specific cell types play in modulating neurophysiological activity across large scale circuits spanning multiple brain areas.

Acknowledgments

We would like to thank L. Oliveira, T. Jones, and G. Wood for miscellaneous support, and S. Halkiotis for proofreading this manuscript. This work was supported by funding from UNCF/Merck, and NIMH grant P50MH060451-09S1 to KD; and by NIH grant R33NSO49534, and The Safra Foundation to MALN. A special thanks to Freeman Hrabowski, Robert and Jane Meyerhoff, and the Meyerhoff Scholarship Program.

References

Adhikari A, Topiwala MA, Gordon JA. Synchronized Activity between the Ventral Hippocampus and the Medial Prefrontal Cortex during Anxiety. Neuron. 2010; 65:257–69. [PubMed: 20152131]

Alexander GM, Rogan SC, Abbas AI, Armbruster BN, Pei Y, Allen JA, Nonneman RJ, Hartmann J, Moy SS, Nicolelis MA, McNamara JO, Roth BL. Remote control of neuronal activity in transgenic mice expressing evolved G protein-coupled receptors. Neuron. 2009; 63:27–39. [PubMed: 19607790]

Buhl DL, Harris KD, Hormuzdi SG, Monyer H, Buzsaki G. Selective impairment of hippocampal gamma oscillations in connexin-36 knock-out mouse in vivo. J Neurosci. 2003; 23:1013–8. [PubMed: 12574431]

Carelli RM, Ijames SG, Crumling AJ. Evidence that separate neural circuits in the nucleus accumbens encode cocaine versus “natural” (water and food) reward. J Neurosci. 2000; 20:4255–66. [PubMed: 10818162]

Costa RM, Lin SC, Sotnikova TD, Gainetdinov RR, Cyr M, Caron MG, MALN. Rapid alterations in corticostriatal ensemble coordination during acute dopamine-dependent motor dysfunction. Neuron. 2006; 52:359–69. [PubMed: 17046697]

Dzirasa, K. Chronic recordings in transgenic mice. In: Nicolelis, MA., editor. Methods for Neural Ensemble Recordings. CRC press: Boca Raton; 2008. p. 83-96.

Dzirasa K, Phillips HW, Sotnikova TD, Salahpour A, Kumar S, Gainetdinov RR, Caron MG, Nicolelis MA. Noradrenergic control of cortico-striato-thalamic and mesolimbic cross-structural synchrony. J Neurosci. 2010a; 30:6387–97. [PubMed: 20445065]

Dzirasa K, Phillips HW, Sotnikova TD, Salahpour A, Kumar S, Gainetdinov RR, Caron MG, Nicolelis MA. Noradrenergic control of cortico-striato-thalamic and mesolimbic cross-stuctural syncrhony. J Neurosci. 2010b In, Press.

Dzirasa K, Ramsey AJ, Takahashi DY, Stapleton J, Potes JM, Williams JK, Gainetdinov RR, Sameshima K, Caron MG, Nicolelis MA. Hyperdopaminergia and NMDA receptor hypofunction disrupt neural phase signaling. J Neurosci. 2009a; 29:8215–24. [PubMed: 19553461]

Dzirasa K, Ribeiro S, Costa R, Santos LM, Lin SC, Grosmark A, Sotnikova TD, Gainetdinov RR, Caron MG, Nicolelis MA. Dopaminergic Control of Sleep-Wake States. J Neurosci. 2006; 26:10577–89. [PubMed: 17035544]

Dzirasa K, Santos LM, Ribeiro S, Stapleton J, Gainetdinov RR, Caron MG, Nicolelis MA. Persistent hyperdopaminergia decreases the peak frequency of hippocampal theta oscillations during quiet waking and REM sleep. PLoS One. 2009b; 4:e5238. [PubMed: 19381303]

Ekstrand MI, Terzioglu M, Galter D, Zhu S, Hofstetter C, Lindqvist E, Thams S, Bergstrand A, Hansson FS, Trifunovic A, Hoffer B, Cullheim S, Mohammed AH, Olson L, Larsson NG. Progressive parkinsonism in mice with respiratory-chain-deficient dopamine neurons. Proc Natl Acad Sci U S A. 2007; 104:1325–30. [PubMed: 17227870]

Fell J, Klaver P, Lehnertz K, Grunwald T, Schaller C, Elger CE, Fernandez G. Human memory formation is accompanied by rhinal-hippocampal coupling and decoupling. Nat Neurosci. 2001; 4:1259–64. [PubMed: 11694886]

Giros B, Jaber M, Jones SR, Wightman RM, Caron MG. Hyperlocomotion and indifference to cocaine and amphetamine in mice lacking the dopamine transporter. Nature. 1996; 379:606–12. [PubMed: 8628395]

Gordon JA, Lacefield CO, Kentros CG, Hen R. State-dependent alterations in hippocampal oscillations in serotonin 1A receptor-deficient mice. J Neurosci. 2005; 25:6509–19. [PubMed: 16014712]

Jones MW, Wilson MA. Theta rhythms coordinate hippocampal-prefrontal interactions in a spatial memory task. PLoS Biol. 2005; 3:e402. [PubMed: 16279838]

Kellendonk C, Simpson EH, Polan HJ, Malleret G, Vronskaya S, Winiger V, Moore H, Kandel ER. Transient and selective overexpression of dopamine D2 receptors in the striatum causes persistent abnormalities in prefrontal cortex functioning. Neuron. 2006; 49:603–15. [PubMed: 16476668]

McHugh TJ, Jones MW, Quinn JJ, Balthasar N, Coppari R, Elmquist JK, Lowell BB, Fanselow MS, Wilson MA, Tonegawa S. Dentate gyrus NMDA receptors mediate rapid pattern separation in the hippocampal network. Science. 2007; 317:94–9. [PubMed: 17556551]

Mohn AR, Gainetdinov RR, Caron MG, Koller BH. Mice with reduced NMDA receptor expression display behaviors related to schizophrenia. Cell. 1999; 98:427–36. [PubMed: 10481908]

Nelson MJ, Pouget P, Nilsen EA, Patten CD, Schall JD. Review of signal distortion through metal microelectrode recording circuits and filters. J Neurosci Methods. 2008; 169:141–57. [PubMed: 18242715]

Nicolelis MA, Dimitrov D, Carmena JM, Crist R, Lehew G, Kralik JD, Wise SP. Chronic, multisite, multielectrode recordings in macaque monkeys. Proc Natl Acad Sci U S A. 2003; 100:11041–6. [PubMed: 12960378]

Nicolelis MA, Ghazanfar AA, Faggin BM, Votaw S, Oliveira LM. Reconstructing the engram: simultaneous, multisite, many single neuron recordings. Neuron. 1997; 18:529–37. [PubMed: 9136763]

Owesson-White CA, Ariansen J, Stuber GD, Cleaveland NA, Cheer JF, Wightman RM, Carelli RM. Neural encoding of cocaine-seeking behavior is coincident with phasic dopamine release in the accumbens core and shell. Eur J Neurosci. 2009; 30:1117–27. [PubMed: 19735286]

Rodriguez E, George N, Lachaux JP, Martinerie J, Renault B, Varela FJ. Perception's shadow: long-distance synchronization of human brain activity. Nature. 1999; 397:430–3. [PubMed: 9989408]

Roybal K, Theobold D, Graham A, DiNieri JA, Russo SJ, Krishnan V, Chakravarty S, Peevey J, Oehrlein N, Birnbaum S, Vitaterna MH, Orsulak P, Takahashi JS, Nestler EJ, Carlezon WA Jr, McClung CA. Mania-like behavior induced by disruption of CLOCK. Proc Natl Acad Sci U S A. 2007; 104:6406–11. [PubMed: 17379666]

Seidenbecher T, Laxmi TR, Stork O, Pape HC. Amygdalar and hippocampal theta rhythm synchronization during fear memory retrieval. Science. 2003; 301:846–50. [PubMed: 12907806]

Svenningsson P, Tzavara ET, Carruthers R, Rachleff I, Wattler S, Nehls M, McKinzie DL, Fienberg AA, Nomikos GG, Greengard P. Diverse psychotomimetics act through a common signaling pathway. Science. 2003; 302:1412–5. [PubMed: 14631045]

Trantham H, Szumlinski KK, McFarland K, Kalivas PW, Lavin A. Repeated cocaine administration alters the electrophysiological properties of prefrontal cortical neurons. Neuroscience. 2002; 113:749–53. [PubMed: 12182882]

Welch JM, Lu J, Rodriguiz RM, Trotta NC, Peca J, Ding JD, Feliciano C, Chen M, Adams JP, Luo J, Dudek SM, Weinberg RJ, Calakos N, Wetsel WC, Feng G. Cortico-striatal synaptic defects and OCD-like behaviours in Sapap3-mutant mice. Nature. 2007; 448:894–900. [PubMed: 17713528]

Zweifel LS, Parker JG, Lobb CJ, Rainwater A, Wall VZ, Fadok JP, Darvas M, Kim MJ, Mizumori SJ, Paladini CA, Phillips PE, Palmiter RD. Disruption of NMDAR-dependent burst firing by dopamine neurons provides selective assessment of phasic dopamine-dependent behavior. Proc Natl Acad Sci U S A. 2009; 106:7281–8. [PubMed: 19342487]

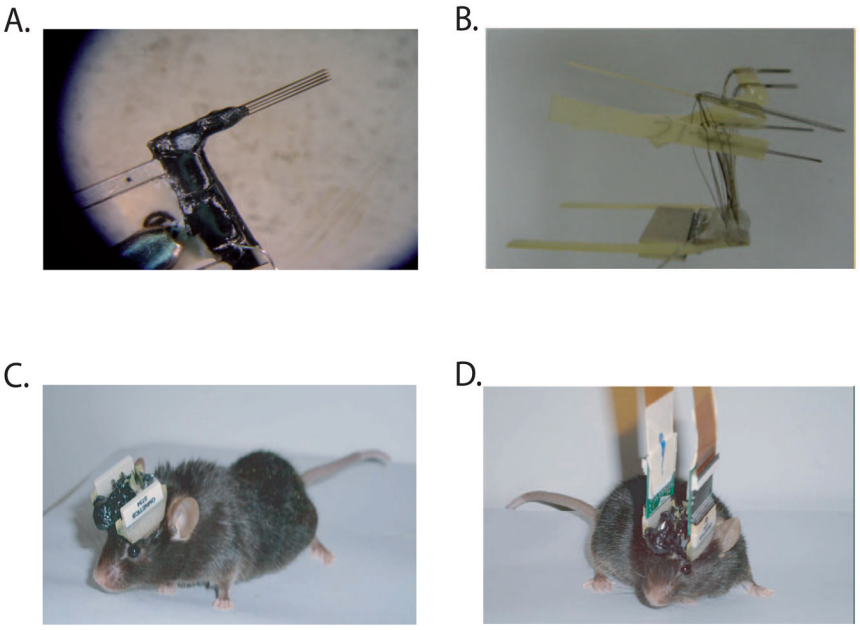

Figure 1. Floating microwire bundle implants

A) Fixed microwire and **B)** Floating microwire bundle electrode designs. Each bundle is fixed to a flat cardboard or plastic holder to aid in surgical implantation. **C)** Adult male mouse implanted with two 32 microwire array bundles. **D)** Full setup can be observed, with two headstage-amplifiers connected to their respective microwire arrays

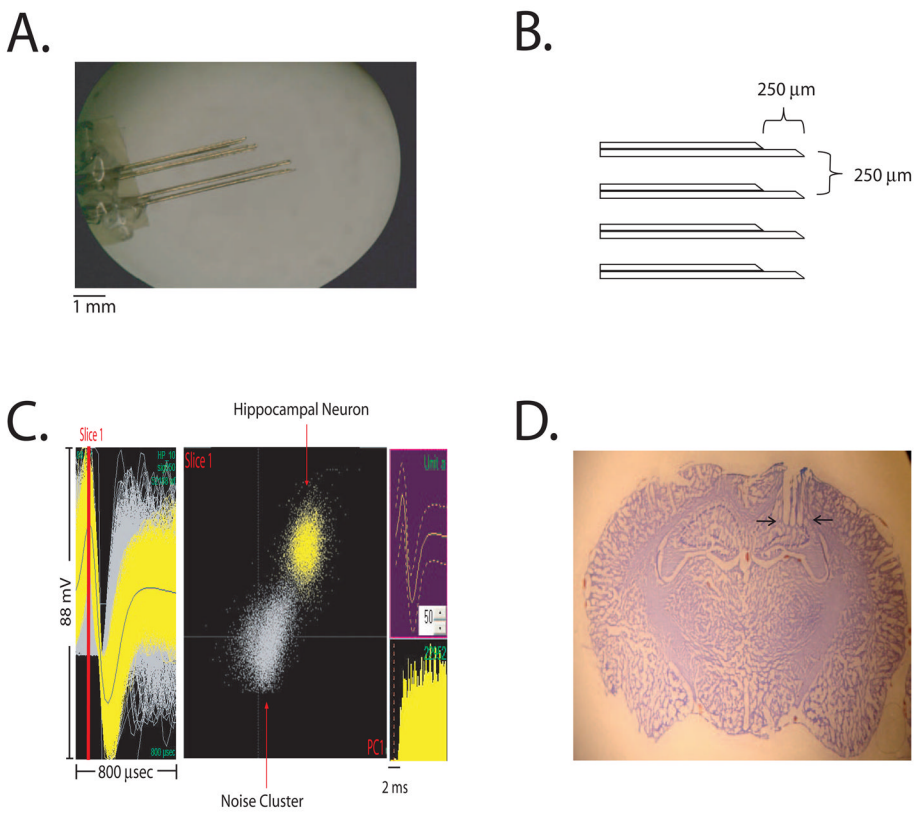

Figure 2. High-density microwire implants

A) Image of 32 30µm diameter microwire array bundle. **B**) Schematic of high-density microwire array tips. **C)** Example of an isolated single unit in Hippocampus. From left to right: depiction of the extracellularly recorded wave forms of the unit (yellow traces); projection of the clusters correspondent to the unit and the noise based on analysis of the first principal component and a peak slice of the waveforms recorded and interspike interval histogram showing a refractory period greater than 1.3ms. **D**) Example lesion tracks for dorsal hippocampal microwire implant.

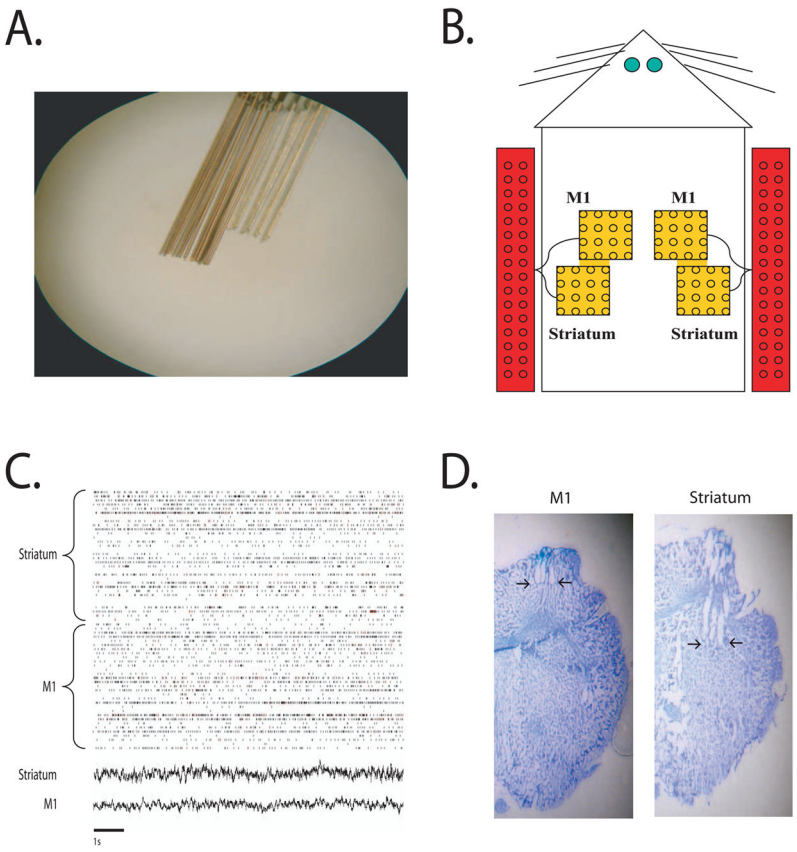

Figure 3. High-density multi-area recordings in mice

A) High-density staggered microwire array designed to target primary motor cortex (M1) and striatum simultaneously. **B**) Schematic of multi-structure implantation strategy representing the head of the animal as seen from above and the relative position of microwire bundles (yellow) and their respective adaptors (red). **C**) Raster plot displaying local field potentials (bottom) and 65 single neurons (top) recorded simultaneously from a freely behaving mouse. D) Example of lesion tracks in M1 and striatum in an animal implanted with multi-structure electrode.

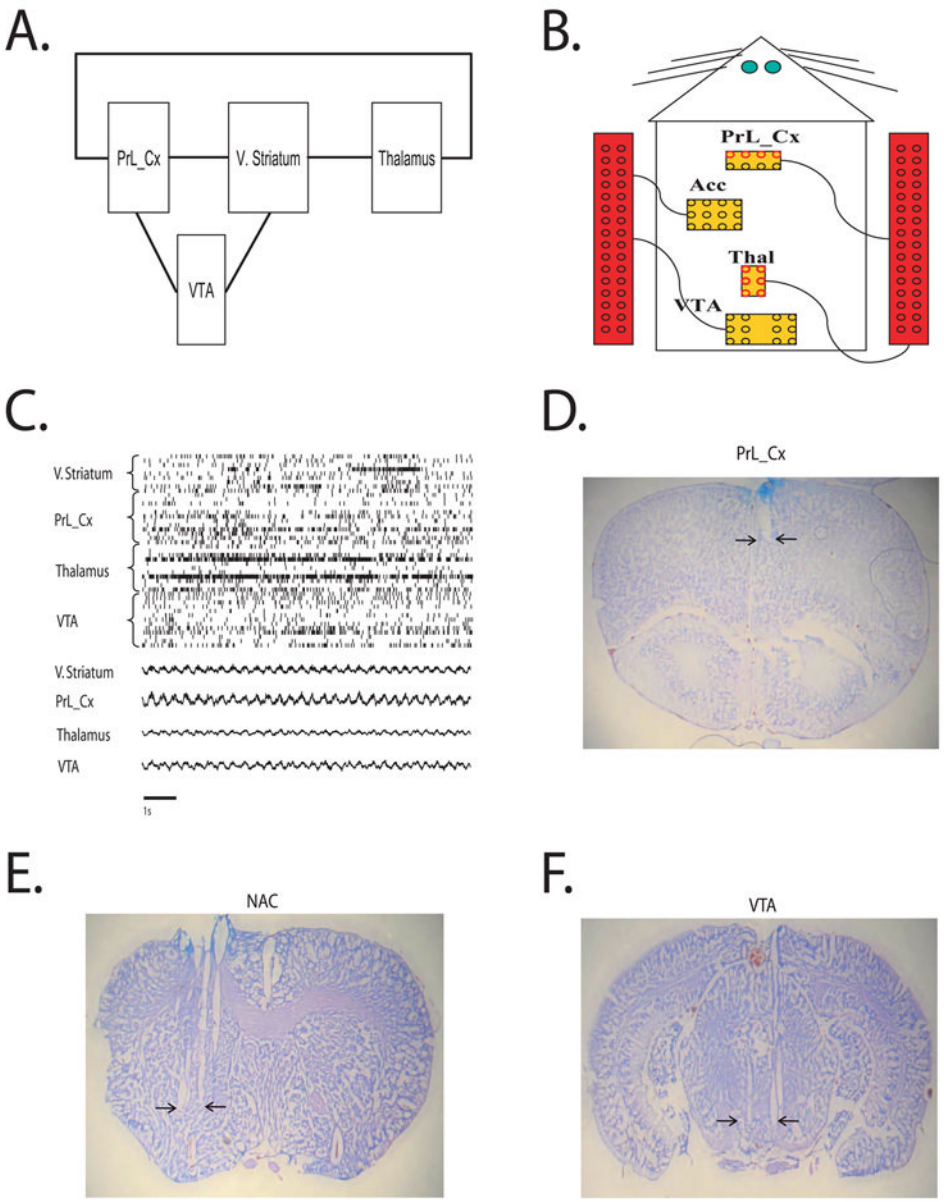

Figure 4. Chronic recordings of large scale neural circuits

A) Schematic of dopamine reward circuit. **B**) Schematic of large scale circuit implantation strategy. Red circles represent two microwires staggered by 250μm, while black circles represent a single microwire. **C**) Raster plot displaying local field potentials and 53 single neurons recorded simultaneously from a freely behaving mouse. **D–F)** Example lesion tracks for PrL_Cx, NAC, and VTA microwire implants. Images depict the AP center of each implanted brain area.

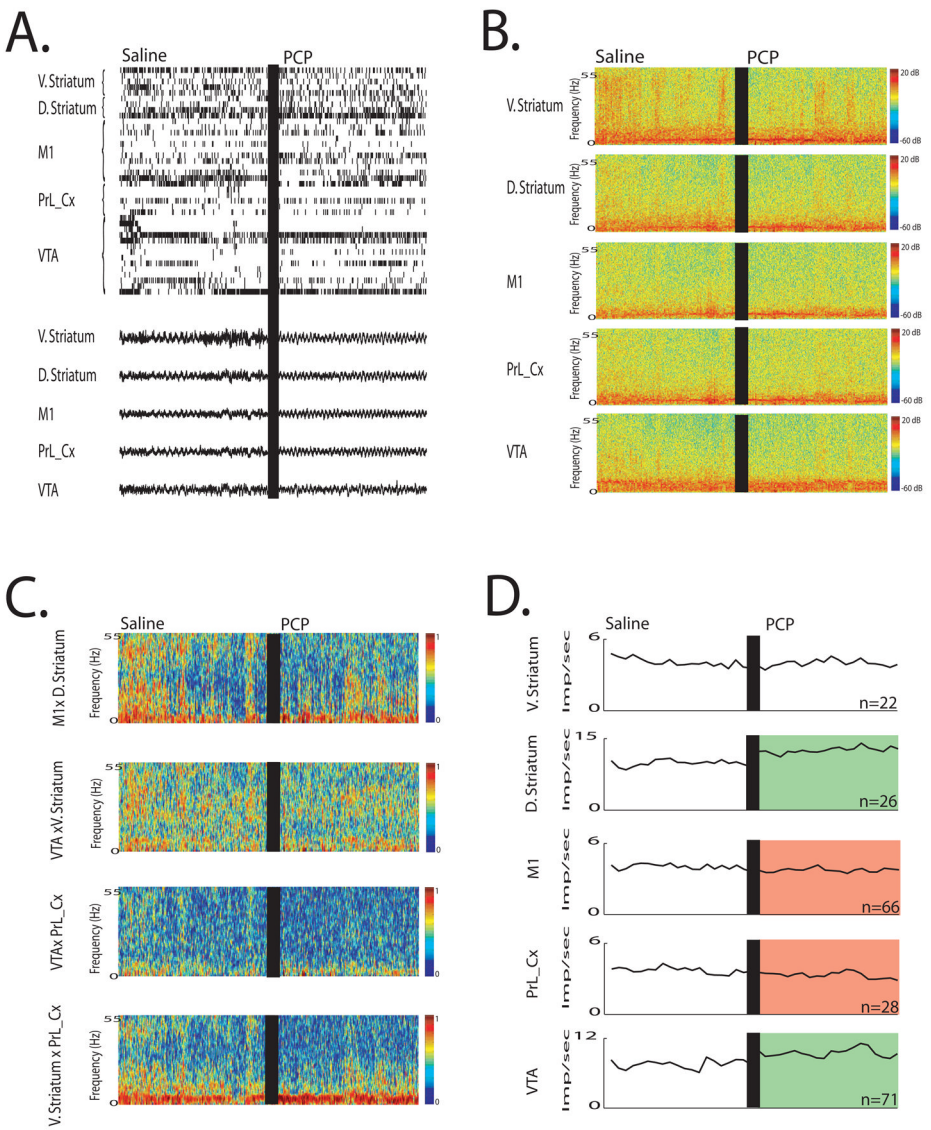

Figure 5. Diverse dopamine reward and motor circuit changes induced by treatment with PCP

A) LFP and single units recorded in the same session following treatment with saline and PCP. **B)** Power spectral plots calculated from LFPs recorded in mice treated with Saline and PCP. **C)** LFP spectral coherence plots generated for LFPs recorded across the dopamine reward and motor circuit. Mice displayed a 1–6Hz, 10–25Hz and 30–55Hz coherence band across the circuits examined. **D)** Treatment with PCP increased the DLS and VTA population firing rate, and reduced the M1 and PrL_Cx population firing rate; $p<0.01$ for all significant comparisons. Green highlights correspond with significant increases, while red highlights correspond with significant decreases in the population firing rate.

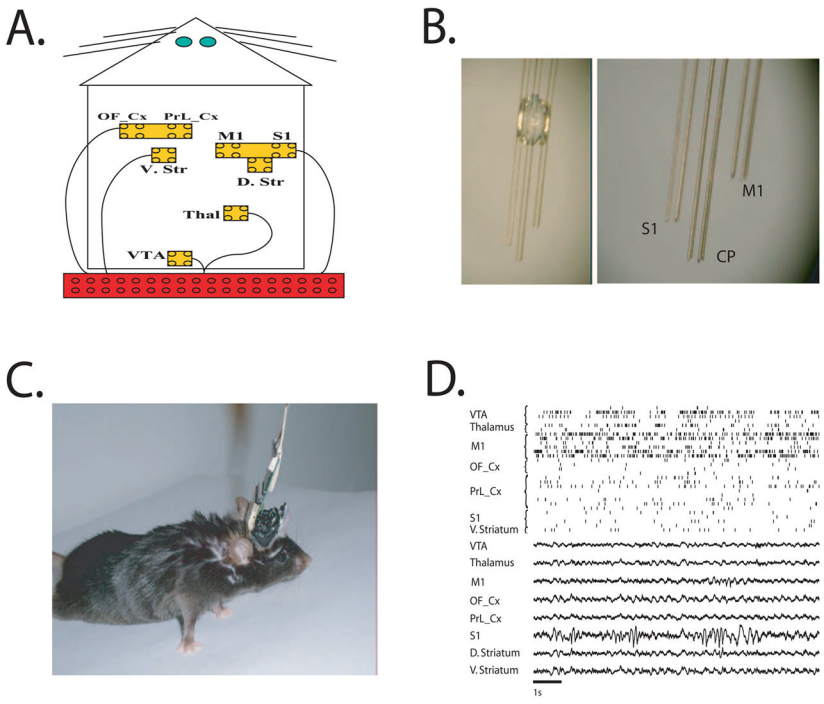

Figure 6. Lightweight multi-circuit recordings in mice

A) Schematic of multi-circuit implantation strategy using one 32 microwire electrode. **B)** Microwire bundle designed to target three brain structures simultaneously. **C)** Mouse implanted across eight areas with a 32 microwire electrode. **D)** Raster plot displaying local field potentials and 29 single neurons recorded simultaneously across eight brain areas in a freely behaving mouse.

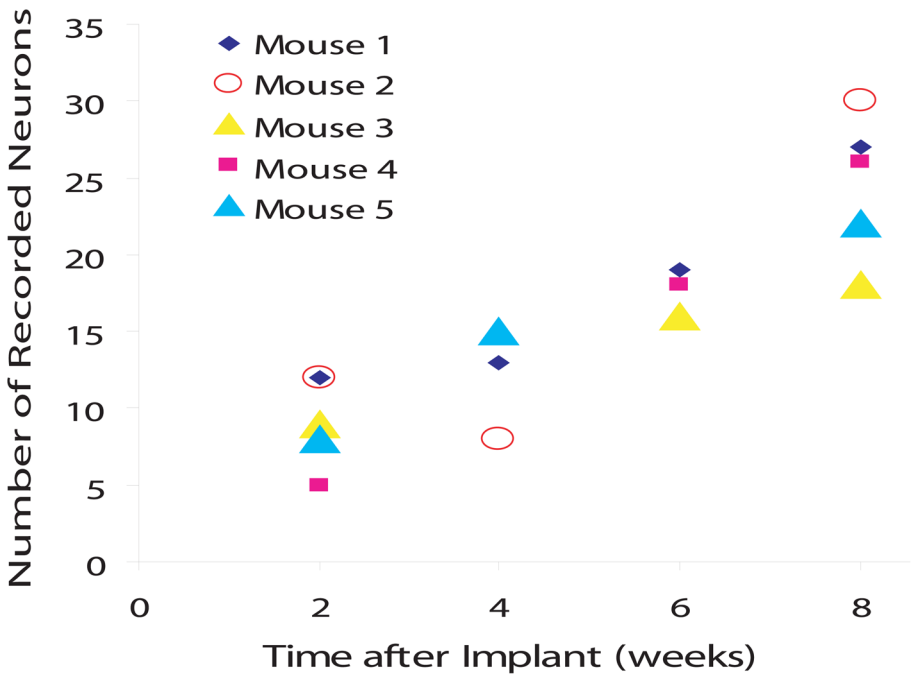

Figure 7.
Neurons isolated across multiple brain circuits during serial recordings in mice

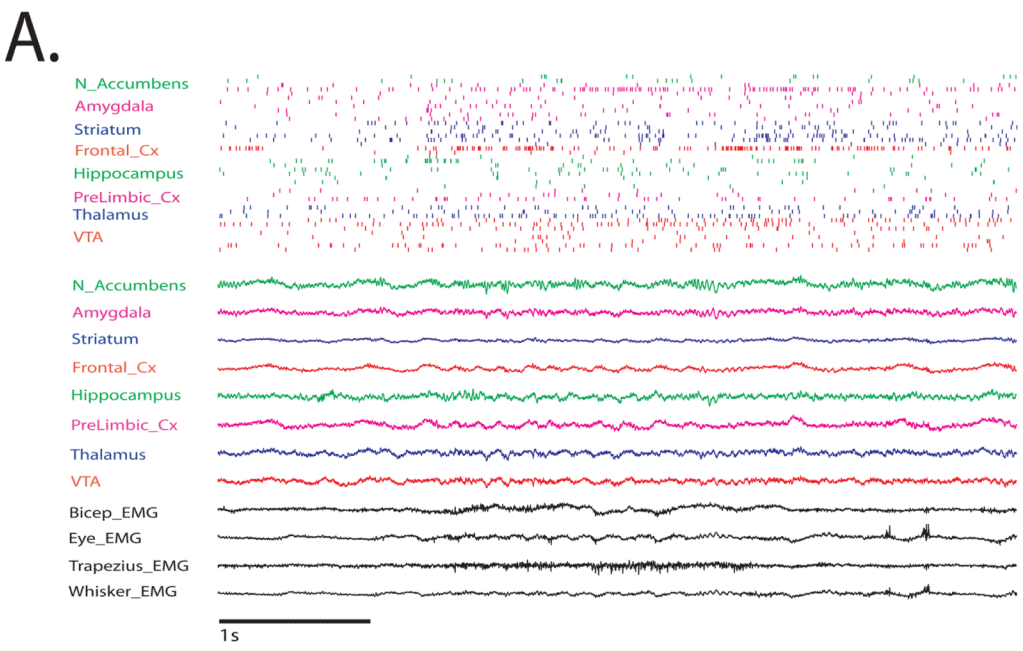

Figure 8.
Simultaneous multi-structure and electromyographic recordings in mice

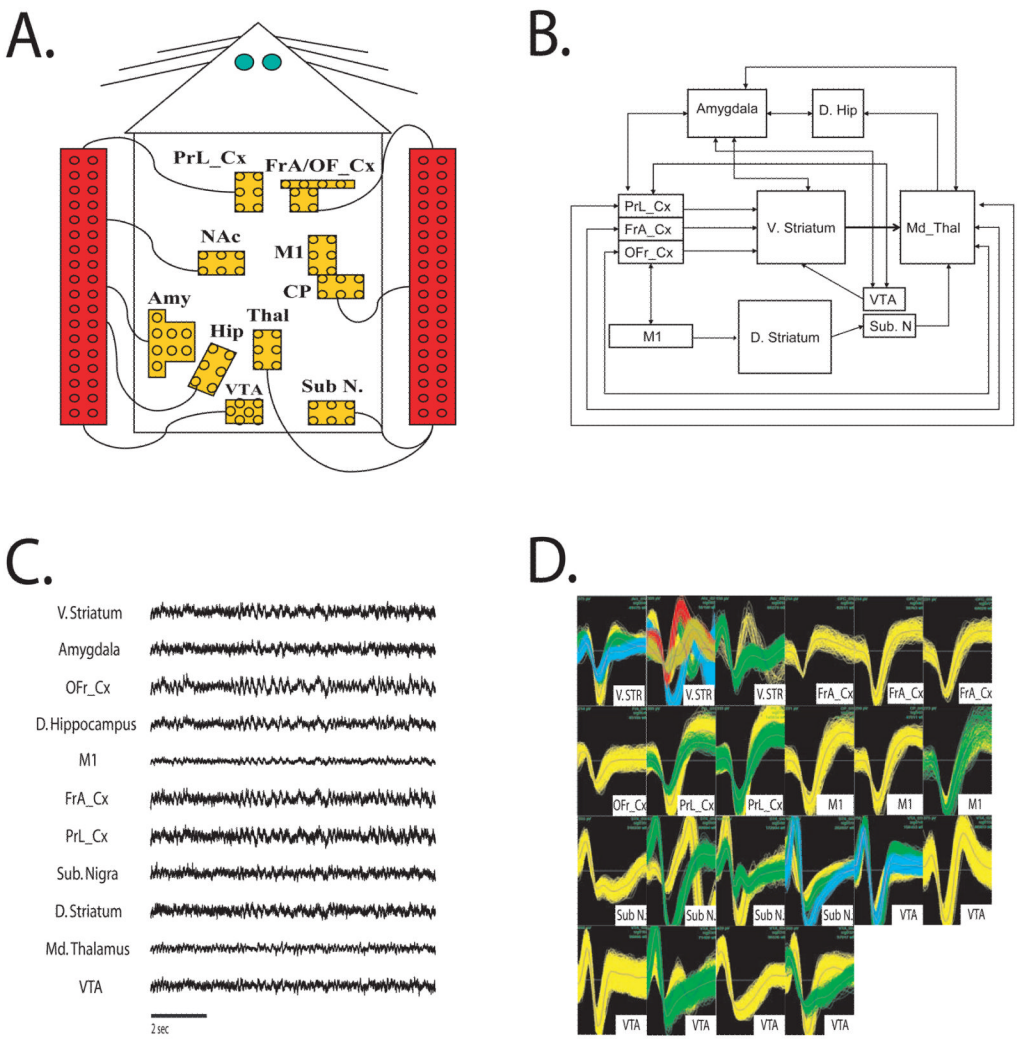

Figure 9. Chronic multi-cell multi-circuit recordings in mice

A) Schematic of multi-circuit implantation strategy using two 32 microwire electrodes. **B)** Schematic of multi-circuit recordings across 11 brain areas. **C)** Local field potentials and **D)** Forty single neurons recorded simultaneously across 11 brain areas.

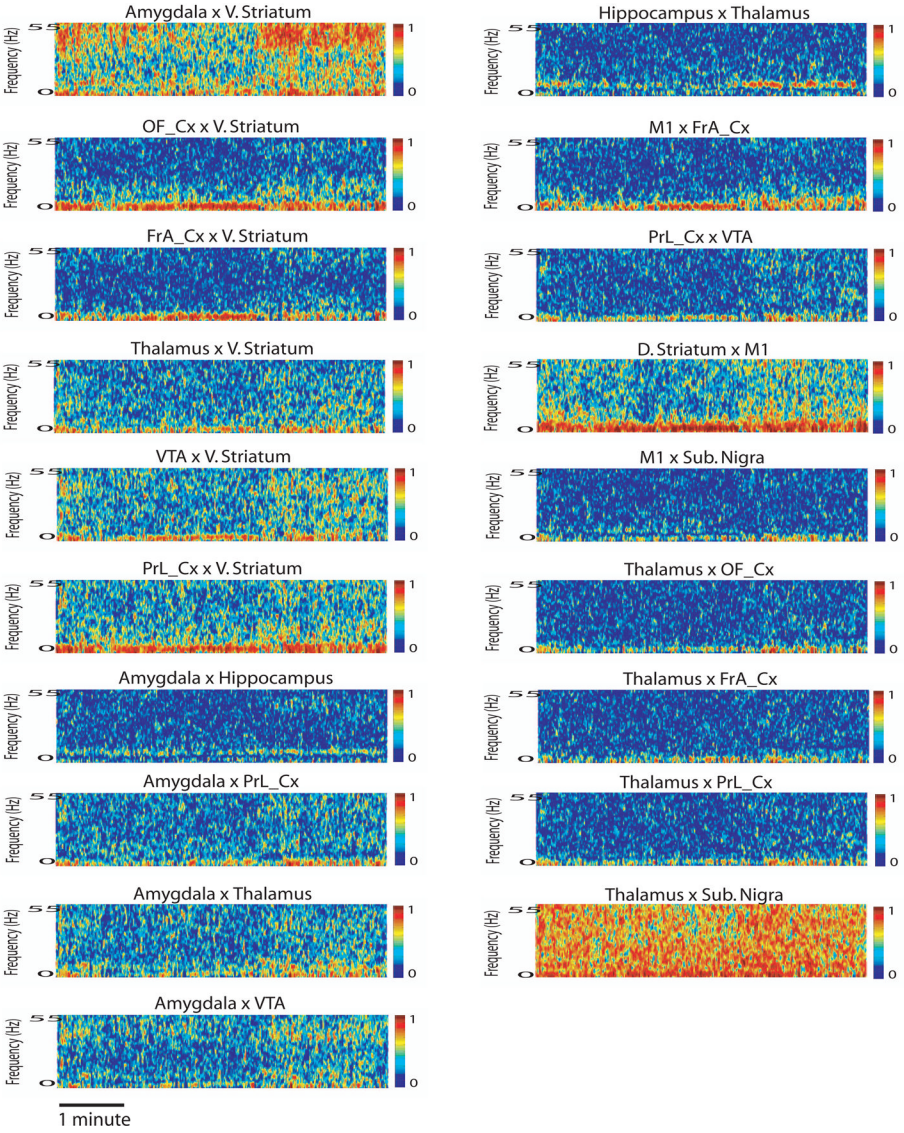

Figure 10. Synchrony across large scale neural circuits in mice

Coherence plots calculated for brain area pairs depicted in Figure 6B. Each coherence plot represents data recorded simultaneously in a freely behaving mouse during a five-minute session in its home cage. High neural synchrony was observed between thalamus and substantia nigra, while low neural synchrony was observed between dorsal striatum and substantia nigra.

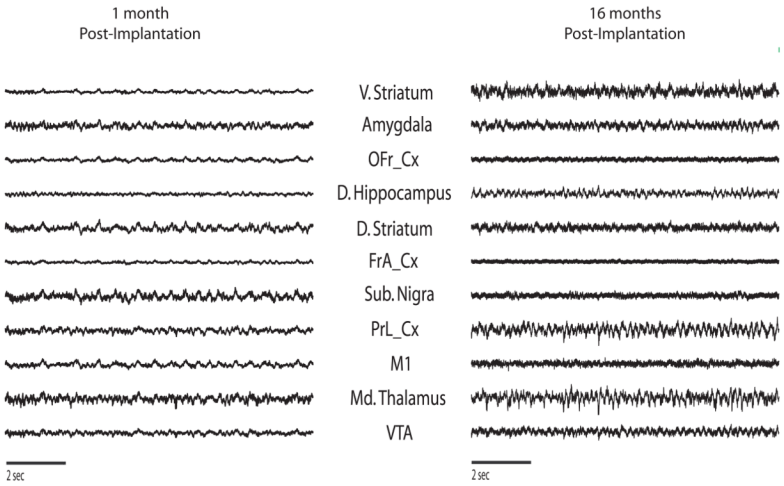

Figure 11. Long-term neural recordings in mice

Local field potentials recorded in the same mouse 1 month (left) and 16 months (right) after surgical implantation.

Table 1

Single neurons isolated from high-density microwire implants.

	Dorsal HP (32 wires)	PrL_Cx (32 wires)	Total
Mouse 1	28	27	**55**
Mouse 2	21	34	**55**
Mouse 3	19	15	**34**
Mouse 4	19	19	**38**
Mouse 5	18	25	**43**
Mouse 6	17	17	**34**
Mouse 7	32	20	**52**
Mouse 8	37	17	**54**
Mouse 9	19	14	**33**
Mouse 10	13	30	**43**
single units/wire	**0.70**	**0.68**	**0.69**

Table 2

Single neurons isolated from multi-structure microwire implants.

	M1 (32 wires)	Striatum (32 wires)	Total
Mouse 1	29	32	**61**
Mouse 2	22	30	**52**
Mouse 3	20	26	**46**
Mouse 4	31	34	**65**
Mouse 5	28	36	**64**
single units/wire	**0.81**	**0.99**	**0.90**

Table 3

Single neurons recorded simultaneously across the dopamine reward circuit.

	V. Striatum (12 wires)	PrL_Cx (16 wires)	Thalamus (12 wires)	VTA (10 wires)	Total (56)
Mouse 1	7	17	7	6	**37**
Mouse 2	2	11	8	12	**33**
Mouse 3	14	6	8	25	**53**
Mouse 4	6	6	1	44	**57**
Mouse 5	9	12	11	13	**45**
Mouse 6	6	6	0	37	**49**
Mouse 7	11	10	5	26	**52**
Mouse 8	17	5	3	48	**73**
Mouse 9	2	3	3	60	**68**
single units/wire	**0.69**	**0.53**	**0.43**	**3.01**	**0.82**

Table 4

Diverse LFP oscillatory power changes induced by treatment with PCP

Table shows power ratio values observed in mice following PCP treatment versus those observed following treatment with saline; n = 6 mice, $p<0.01$ for all significant comparisons using paired t-test; green highlights correspond with significant increases, while red highlights correspond with significant decreases in the population firing rate.

	1–4Hz	4–8Hz	8–14Hz	14–30Hz	30–55Hz
V. Striatum	*1.42 ± 0.12	*1.39 ± 0.11	1.12 ± 0.11	0.92 ± 0.04	*0.66 ± 0.05
D.L. Striatum	1.42 ± 0.17	*1.29 ± 0.08	1.07 ± 0.08	*0.92 ± 0.02	*0.85 ± 0.03
M1	1.29 ± 0.40	*1.27 ± 0.08	1.22 ± 0.12	0.97 ± 0.04	*0.94 ± 0.02
PrL_Cx	1.37 ± 0.17	*1.26 ± 0.10	1.31 ± 0.18	0.99 ± 0.03	0.99 ± 0.05
VTA	1.40 ± 0.25	*1.22 ± 0.08	1.07 ± 0.07	*0.90 ± 0.03	0.94 ± 0.03

Table 5

Diverse dopamine reward and motor circuit changes induced by treatment with PCP

Table shows LFP spectral coherence ratio values observed in mice following PCP treatment versus those observed following treatment with saline; n = 6 mice, $p<0.01$ for all significant comparisons using paired t-test; green highlights correspond with significant increases, while red highlights correspond with significant decreases in the population firing rate.

	1–6Hz	10–25Hz	30–55Hz
D. L. Striatum x M1	1.00 ± 0.05	1.02 ± 0.04	*0.78 ± 0.05
V. Striatum x Prl_Cx	*1.13 ± 0.04	1.03 ± 0.07	*0.70 ± 0.07
PrL_Cx x VTA	*1.24 ± 0.06	1.05 ± 0.09	*0.73 ± 0.07
VTA x V. Striatum	*1.14 ± 0.03	1.02 ± 0.06	*0.84 ± 0.06

Table 6

Single neurons isolated from thirty-two wire multi-circuit implant

	OFC	VTA	M1	Acb	PrL	Thal	S1	CP	Total (32)
Mouse 1	4	3	2	0	2	1	0	0	12
Mouse 2	0	2	3	0	0	1	3	0	9
Mouse 3	1	3	1	0	0	0	3	1	9
Mouse 4	2	3	0	0	3	0	4	0	12
Mouse 5	2	3	1	0	2	0	3	0	11
single units/wire	**0.45**	**0.70**	**0.35**	**0**	**0.35**	**0.10**	**0.65**	**0.05**	**0.66**

Table 7

Single neurons isolated in freely behaving mice more than a year after surgical implantation.

	1 month	13–16 months
Mouse 1	27	15
Mouse 2	39	30